Nonintrusive monitoring and quantitative analysis of strong laser-field-induced impulsive alignment

V. Renard, M. Renard, A. Rouzée, S. Guérin, H. R. Jauslin, B. Lavorel, and O. Faucher
Laboratoire de Physique de l'Université de Bourgogne, UMR CNRS 5027, BP 47870, 21078, France
(Received 1 April 2004; published 30 September 2004)

We report the observation of impulsive alignment of CO_2 molecules produced through their interaction with a nonresonant, strong laser pulse. The periodic alignment is monitored using a polarization technique generally employed in optical Kerr effect experiments; the birefringence produced by alignment of the molecular sample is measured with a weak pulse, time-delayed with respect to the alignment pulse. The technique provides a signal proportional to $\langle\cos^2\theta\rangle-\frac{1}{3}$, where θ is the polar angle between the molecular axis and the strong-field polarization axis. Experiments are conducted at room and at low temperatures. Two methods of analysis are presented. The first one consists in comparing the signal with the prediction of the time-dependent Schrödinger equation. From a fine analysis of the temporal signal shape one can then deduce the value of $\langle\cos^2\theta\rangle$. The second one allows us to extract $\langle\cos^2\theta\rangle$ through a calibration of the birefringence signal obtained by performing the experiment in a reference atomic gas sample. Both analyses are compared and found in good agreement for the different laser intensities investigated. Saturation of the alignment process is observed at a laser intensity that agrees with the ionization saturation intensities of CO_2.

DOI: 10.1103/PhysRevA.70.033420 PACS number(s): 42.50.Hz, 32.80.Lg, 33.80.−b, 42.50.Md

I. INTRODUCTION

The manipulation of the external degrees of freedom of a molecule with light is a topic of growing interest. The idea of manipulating molecules in space generates indeed stimulating perspectives in fields ranging from (i) chemistry and surface processing, through (ii) nonlinear optics [1], and more generally strong-field molecular physics like high harmonic generation [2] and strong-field ionization [3,4], to (iii) molecular optics and nanoscience technology [5,6]. In all of these areas, angularly squeezed states and/or molecular focusing and molecular trapped states play a key role. It is now well established that a polyatomic molecule submitted to a strong electromagnetic field, as commonly produced by short laser pulses, can experience, among other effects, a torque on at least one of its axes resulting in an alignment, i.e., angular localization, of the molecule in space (see Ref. [7] for a review). This is encountered when a nonspherical top molecule interacts with a nonresonant laser pulse. The interaction of the electric field vector with the molecular polarizability imposes on the molecule an angular potential that converts the free rotation of the system to confined angular displacements. In the case of a linear molecule exposed to a linearly polarized laser field the effective interaction Hamiltonian depends on only one angle θ, the polar angle, among the three Euler angles of rotation (φ,θ,χ) that describe the orientation of the molecule in the space-fixed frame. This type of interaction leads to one-dimensional alignment of the molecule in a sense that the two other Euler angles, φ and χ, are not confined. In general, an elliptically polarized field applied on an asymmetric top molecule will result in a three-dimensional alignment of the molecule [8]. It is noted that the molecular polarizability is also responsible for the deflection of the molecule in the field gradient that occurs simultaneously with the alignment [9].

The present work concerns the quantitative characterization of laser-induced one-dimensional alignment, referred throughout the paper as alignment, of the linear CO_2 molecule. Dealing with alignment under short laser pulses, one must distinguish between the two regimes under which alignment is conventionally achieved: adiabatic [6,10–13] and impulsive (postpulse) [12,14–19] alignment. Typically, adiabatic alignment is produced with a strong laser field of duration much longer than the rotational period of the molecule. The alignment exists only during the laser pulse, reaching its optimal value at the maximum field. After turn-off of the field, the alignment disappears as the molecule returns to its initial rotational state. Impulsive or postpulse alignment leads to alignment in the field-free conditions, either immediately after a short strong pulse [19], or at a subsequent revival of the rotational wave packet. The advantage of the latter is that the strongly aligned molecules that can be produced in field-free conditions are generally more suitable for applications. The drawback is the short time, typically of the order of a few picoseconds, during which the molecules are effectively aligned. With the adiabatic regime the alignment is maintained during several nanoseconds. Finally, we mention the scheme first proposed by T. Seideman [14], which is a mixture of adiabatic and impulsive regimes. It is based on the use of shaped laser pulses designed to optimize the field-free alignment. A laser pulse with a long turn-on and a sudden turn-off will adiabatically align the molecule during the rising time of the pulse, whereas the abrupt falling edge of the pulse will leave the molecule in a broad rotational wave packet, whose recurrence leads to an efficient alignment under field-free conditions. Recently, this idea has been applied for N_2 and CO_2, where a "switched wave packet" has been produced experimentally [20].

In a recent paper [21], we have reported the observation of postpulse molecular alignment using an experimental method that allows quantitative evaluation of the alignment. The aligned molecules were probed with a polarization technique involving a weak laser field that itself does not pro-

duce appreciable alignment, nor ionization. For this reason the technique can be considered nonintrusive. It can operate for large number densities and allows us to produce and monitor alignment of bulk molecules that is suitable for high harmonic generation, gas-surface interaction, and chemical processes. The present work completes the former studies, reporting experimental results, recorded at room and at low temperatures. We also discuss a theoretical model that provides approximate analytical solutions. In addition, a part of the paper is dedicated to the calibration of measurements, where we implement a technique that allows monitoring of the alignment at different laser intensities without numerical simulation.

II. THEORY

The experimental setup described in the next section is commonly used in pump-probe polarization spectroscopy [22]. It is arranged for measuring the transient birefringence of a gas sample consecutive to its interaction with a linearly polarized pump-field. The field-induced birefringence is accessed by measuring the ellipticity of an initially linearly polarized probe-field traveling through the nonlinear medium. In the weak signal-field limit with a probe-field polarized at 45° with respect to the pump-field direction, the birefringence signal S is given by

$$S(t) = \kappa[\Delta n(t) + C]^2, \tag{1}$$

where

$$\Delta n(t) = n_{\parallel}(t) - n_{\perp}(t) \tag{2}$$

is the difference of refractive indices (at the probe frequency) between the parallel ($\parallel$) and any perpendicular ($\perp$) direction of the pump polarization axis. κ is a factor that accounts for the probe-field intensity, the geometry of the beams, and the detection efficiency. The constant C corresponds to any additional birefringence, other than the one introduced by the molecule itself, and is only used in case of heterodyne detection. For atoms, the induced birefringence only results from the quasi-instantaneous deformation of the electronic cloud and one usually writes

$$\Delta n(t) = \overline{n_2} I(t), \tag{3}$$

as the first term of a power series in the pump-laser intensity I, with $\overline{n_2}$ the difference of the nonlinear refractive indices. For molecules, the induced birefringence results from the electronic and/or nuclear excitation but also from the alignment or the orientation of the molecular axis. The latter contribution leads to a refractive index difference that depends on the average value of $\cos^2\theta$ through the expression [23]

$$\Delta n(t) = \frac{3N\Delta\alpha}{4n\epsilon_0}\left(\langle\cos^2\theta\rangle(t) - \frac{1}{3}\right), \tag{4}$$

where n is the average value of the refractive index at the probe frequency, N is the number density, ϵ_0 is the dielectric constant of vacuum, and $\Delta\alpha = \alpha_{\parallel} - \alpha_{\perp}$ is the polarizability anisotropy, with $\alpha_{\parallel}$ and $\alpha_{\perp}$ the components of the dynamical polarizability respectively parallel and perpendicular to the molecular axis. Higher-order polarizabilities (i.e., hyperpolarizabilities) are neglected in Eq. (4).

In this expression the alignment is characterized by the time dependent average (see, e.g., [12])

$$\langle\cos^2\theta\rangle(t) \equiv \sum_{J_0=0}^{\infty} \rho_{J_0} \sum_{M_0=-J_0}^{J_0} \langle\cos^2\theta\rangle_{J_0,M_0}(t) \tag{5}$$

of a statistical ensemble of molecules at temperature T distributed according to the Boltzmann weights ρ_{J_0}, where $\langle\cos^2\theta\rangle_{J_0,M_0}(t)$ is determined for a molecule initially in the state J_0, M_0. We consider a linear molecule in its ground vibronic state, such that one can approximate its Hamiltonian H_0 as a rotor of rotational constant B with a centrifugal distorsion of constant D

$$H_0 = BJ^2 - DJ^4. \tag{6}$$

The molecule is subject to a nonresonant pump laser field

$$\vec{\mathcal{E}}_p(t) = \vec{e}_p \mathcal{E}_0 \sqrt{\Lambda_p(t)} \cos\omega_p t \tag{7}$$

of frequency ω_p, pulse intensity envelope $0 \leqslant \Lambda_p(t) \leqslant 1$ centered at $t=0$ and of duration T_p, peak amplitude $\mathcal{E}_0$ and fixed polarization vector $\vec{e}_p$. Since no excited electronic states and vibrational states are resonantly coupled, one can extract a first effective Hamiltonian [6,24]

$$H = H_0 - \vec{\mu}_p \cdot \vec{\mathcal{E}}_p(t), \tag{8}$$

where for nonpolar molecules (which are considered in this paper) the effective dipole moment is given by

$$\vec{\mu}_p = \frac{1}{2}\vec{\vec{\alpha}}\vec{\mathcal{E}}_p(t), \tag{9}$$

with $\vec{\vec{\alpha}}$ the dynamical polarizability tensor, which includes the contribution of the excited electronic states. If we consider low frequencies with respect to the excited electronic states, the dynamical polarizabilities are well approximated by the static ones. In the high frequency limit (with respect to the rotational frequency), this leads to the final effective Hamiltonian of second order in the pump field amplitude (in units of B) [6,25]

$$H_{\mathrm{eff}}/B = H_0/B - \Lambda_p(t)(\Delta\gamma\cos^2\theta + \gamma_{\perp}) \tag{10}$$

with

$$\gamma_{\perp} = \frac{\mathcal{E}_0^2}{4B}\alpha_{\perp},\ \Delta\gamma = \frac{\mathcal{E}_0^2}{4B}\Delta\alpha. \tag{11}$$

The dynamics in a strong nonresonant pump field are described by a state vector $\phi(t)$, solution of the time-dependent Schrödinger equation $i\hbar\partial\phi(t)/\partial t = H_{\mathrm{eff}}\,\phi(t)$ with as initial condition at $t=t_i$ a pure state eigenvector of H_0: $\phi_{J_0,M_0}(t=t_i) = |J_0, M_0\rangle$. After the pump excitation, switched off at $t=t_f$, the state vector of the free molecule evolves as

$$\psi_{J_0,M_0}(t > t_f) = \exp[-iH_0(t-t_f)/\hbar]\phi_{J_0,M_0}(t_f). \tag{12}$$

Since we consider a linearly polarized pump laser, the coupling does not depend on the azimutal angle $\varphi \in [0, 2\pi[$ and

the quantum number M_0 is preserved during the pump interaction: $\psi_{J_0,M_0}(\theta,\varphi,t)=\phi_{J_0,M_0}(\theta,t)\exp(iM_0\varphi)$ which gives $\langle\cos^2\theta\rangle_{J_0,M_0}(t)=\langle\cos^2\theta\rangle_{\phi_{J_0,M_0}(t)}$.

After interaction with the field, one can expand the state solution as

$$|\psi_{J_0,M_0}(t)\rangle=\sum_J c_J^{J_0,M_0}e^{i[D(J(J+1))^2-BJ(J+1)]t/\hbar}|J,M_0\rangle \quad (13)$$

with

$$c_J^{J_0,M_0}=|c_J^{J_0,M_0}|e^{i\theta_J^{J_0,M_0}},\ \sum_J|c_J|^2=1. \quad (14)$$

The Hamiltonian (10) shows that the populated J are all either odd or even since only the matrix elements $\alpha_{J,M_0}=\langle J,M_0|\cos^2\theta|J,M_0\rangle$ and $\beta_{J,M_0}=\langle J+2,M_0|\cos^2\theta|J,M_0\rangle$ are different from zero. One can calculate the quantity characterizing the alignment, neglecting the centrifugal distorsion for simplicity

$$\langle\cos^2\theta\rangle_{J_0,M_0}(t)=\sum_J\alpha_{J,M_0}|c_J^{J_0,M_0}|^2+2\sum_J\beta_{J,M_0}|c_J^{J_0,M_0}c_{J+2}^{J_0,M_0}|\times\cos(\omega_J t+\Delta\theta_J^{J_0,M_0}) \quad (15)$$

with the quantum beat phase

$$\Delta\theta_J^{J_0,M_0}=\theta_J^{J_0,M_0}-\theta_{J+2}^{J_0,M_0}, \quad (16)$$

$\omega_J=2B(2J+3)/\hbar$ the Raman frequency, α_{J,M_0} the Stark shift of the $|J,M_0\rangle$ state, and β_{J,M_0} the coupling $|J,M_0\rangle\rightleftharpoons|J+2,M_0\rangle$. Equation (15) shows that each J-component of $\langle\cos^2\theta\rangle_{J_0,M_0}(t)$ oscillates periodically with period $\pi\hbar/[B(2J+3)]$, and thus that $\langle\cos^2\theta\rangle_{J_0,M_0}(t)$ oscillates with the common period $T_r=\pi\hbar/B$, the classical rotational period of the molecule. The average $\langle\cos^2\theta\rangle_{J_0,M_0}(t)$ oscillates around the quantity $\Sigma_J\alpha_{J,M_0}|c_J|^2$ which corresponds to the mean alignment (permanent alignment).

The rephasing of the rotational wave packet and thus transient significant alignment will occur (i) for a given initial condition J_0, M_0 if the phase $\Delta\theta_J^{J_0,M_0}$ is independent of J, and (ii) at any temperature if the phase $\Delta\theta_J^{J_0,M_0}$ is additionally independent of the initial condition characterized by J_0, M_0. In this case, there are four main transient peaks of alignment in one period, called revivals [26]. It is well known that the revivals occur around $t_n=n\pi\hbar/4B=nT_r/4$, $n=1,\ldots,4$. The first (at t_1) and third (at t_3) peaks show, respectively, a minimum (maximum) and a maximum (minimum) if even (odd) J_0 are considered. Around the second (fourth) peak [around t_2 (t_4)], one has a maximum (minimum) located at $t\lesssim t_2$ ($t\lesssim t_4$) and a minimum (maximum) at $t\gtrsim t_2$ ($t\gtrsim t_4$). The functional dependence of ω_J on J_0 is the essential property that determines whether a given peak is a maximum or a minimum for odd or even J_0.

Adding the small centrifugal diagonal term in Eq. (15) will slightly change the frequency ω_J of the oscillations, which will shift the revivals more significantly for larger times.

Numerics shows the additional following features:

(i) At low temperature, the highest peak of $\langle\cos^2\theta\rangle$ as a function of time occurs around t_2 (for a sufficiently high intensity pulse area), it is the highest for $J_0=0$.

(ii) At higher temperature, the highest peak of $\langle\cos^2\theta\rangle$ as a function of time occurs at t_3 (t_1) if even (odd) J_0 are considered (for a sufficiently high intensity pulse area).

(iii) The phases $\Delta\theta^{J_0,M_0}$ are approximately $\pm\pi/2$, which is also the case in the perturbative regime. This allows us to explain the positions of the revivals. Moreover, the contributions of $-\pi/2$ for the phases $\Delta\theta^{J_0,M_0}$ dominate with respect to the ones with $+\pi/2$, which permits efficient revival peaks. In the appendix, we calculate in a solvable model the phase $\Delta\theta_J^{J_0,M_0}$.

Having that $\Delta\theta^{J_0,M_0}\approx\pm\pi/2$, Eq. (15) implies that the positions of the peaks of $\Sigma_{M_0=-J_0}^{J_0}\langle\cos^2\theta\rangle_{J_0,M_0}$ depend on J_0 around t_2 and t_4, and are independent of J_0 at t_1 and t_3. This gives an argument why at high temperature where many J_0 contribute, the highest peak of $\langle\cos^2\theta\rangle$ as a function of time can occur at t_3.

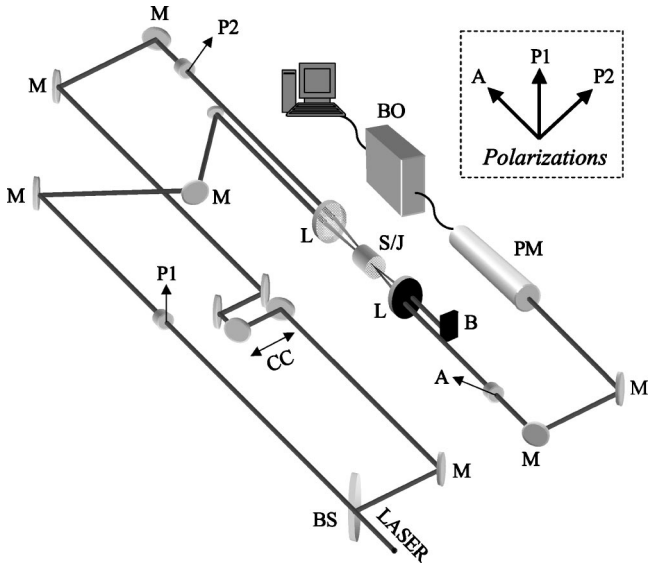

FIG. 1. Experimental setup. M: mirror, BS: beam splitter, L: lens, CC: corner cube, P: polarizer, A: analyzer, B: beam stop, S/J: static or jet cell, PM: photomultiplier, BO: boxcar. The relative polarizations of the pump (P1), probe (P2), and signal-field (A) are shown in the inset.

III. EXPERIMENTAL SETUP

Impulsive alignment is investigated under two experimental conditions: (a) at room temperature, in a static cell, and (b) at low temperature, in a supersonic expansion of a pulsed molecular jet. The setup is shown Fig. 1. In both studies the optical arrangement is the same, consisting of a chirped pulsed amplified Ti:sapphire femtosecond laser with 90 fs pulse duration. The laser is operated at 20-Hz repetition rate with a spectrum centered at 800 nm. The laser beam is split in two parts with 98% of the total energy used in the pump-beam, the 2% left over being used for the probe-beam. The temporal delay between the pump- and the probe-pulse is adjusted by means of a corner cube retroreflector mounted on a motorized linear stage. Both electric fields (pump and

probe) are linearly polarized with an angle of 45° between their respective directions. The two incoming beams are focused by a 17.5-cm focal length and then intersected at a small angle into the interaction gas region. The beam waist, measured by a charge-coupled device camera, is, respectively, 30 and 50 μm for the pump- and probe-beam. A third polarizer, oriented at 90° with respect to the direction of the incoming probe-field, is located at the exit slot of the experimental chamber. It is used to analyze the depolarization of the outgoing probe-field, i.e., the signal-field. The different polarization directions are depicted in the inset of Fig. 1. The signal-field is detected by a photomultiplier, sampled by a boxcar integrator, and finally acquired by a computer. The latter is used also to drive the optical delay line during data acquisition.

The experiment conducted at room temperature is performed in a 0.2-m-long static cell maintained under a pressure of 0.15 bar. A supersonic free jet is used for the investigations conducted at low temperature. The magnetic valve operates at 7-bar backing pressure. It is equipped with a nozzle of 0.5-mm diameter synchronized at 20 Hz with the laser. The laser beams, oriented at a right angle with the jet axis, interact at 1.5 mm from the nozzle. For this distance, one can reasonably assume an isentropic expansion [27] and thus one can estimate the rotational temperature and the number density around 60 K and 2.0×10^{18} cm^{-3}, respectively.

Homodyne and heterodyne detection are used, depending on the experimental conditions. The static cell allows us to perform homodyne detection, the small birefringence of the thin windows being compensated by a wave plate inserted on the optical path of the probe-beam, just after the exit slot of the cell. It is made from a fused silica piece put under mechanical stress. The resulting induced birefringence can be controlled in magnitude, by the amount of mechanical stress, and in sign, by rotation of the plate around the propagation direction. The vacuum chamber used in the low temperature experiment is equipped with thick windows that do not allow a correct compensation of the birefringence. The detection performed in the jet configuration is hence heterodyned. It means that the measured signal includes a local oscillator in phase quadrature with the probe-field [28].

IV. RESULTS AND DISCUSSION

In a recent paper [21] we demonstrated that impulsive alignment can be characterized by a polarization technique using an arrangement like the one described in the preceding section. In particular we showed that the polarization signal, resulting from the birefringence of the molecular sample induced by a strong laser field, is proportional to the degree of molecular alignment and hence to $\left(\langle\cos^2\theta\rangle-\frac{1}{3}\right)$. In the present paper, we explore two methods that allow us to extract $\langle\cos^2\theta\rangle$ from the experimental data. The first one is based on the simulation of the time-dependent Schrödinger equation. The numerical result of this simulation is fitted to the experimental data. Only two parameters are used for the numerical adjustment: a scale factor and an intensity parameter adjusted to a value close to the measured laser intensity.

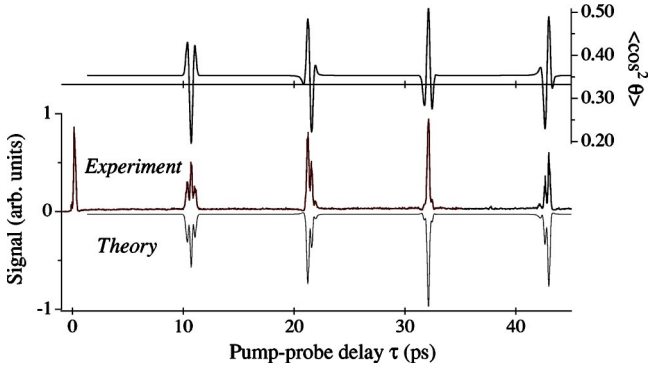

FIG. 2. Lower graph: homodyne signal *(experiment)* versus pump-probe delay τ recorded in CO_2 at 0.15 bar. Numerical simulation *(theory)* of Eq. (1) for a peak intensity of 40 TW/cm^2 (plotted upside down). Upper graph: the corresponding value of $\langle\cos^2\theta\rangle$.

The $\langle\cos^2\theta\rangle$ is obtained from the numerical simulation for the parameters at which the temporal shapes of the calculated and experimental signal coincide (at a given precision). We will refer to this method throughout the paper as the *shape based analysis* method. The second one, named the *relative calibration* method, consists in a calibration of the polarization field detection with respect to the variation of the refractive-index. It is achieved by comparing the optical Kerr effect resulting from the alignment of a molecular sample with the one produced by the electronic response of an atomic gas, illuminated with a short pulse of the same duration.

A. Shape based analysis

Figure 2 displays the polarization signal versus the pump-probe delay measured at room temperature in CO_2 with homodyne detection. The experiment is performed in a static cell using a pump-laser intensity of 56 TW/cm^2. The temporal trace is characterized by transients equally spaced by $T_r/4$ (see Sec. II), with $T_r\approx42.7$ ps. Each transient corresponds to a revival of the rotational wave packet formed by the short pump-pulse. It can be associated either with alignment of the molecule along the field axis or with planar delocalization of the molecule in the equatorial plane, depending on whether $\langle\cos^2\theta\rangle$ is larger or smaller than 1/3, respectively. The signal recorded close to the zero delay results from the quasi-instantaneous electronic response (compared to the pulse duration) combined with the rotational retarded response of the molecule. The convolution of the two contributions results in a transient signal occurring just after the pump-field interaction peak. The nonzero background signal observed between recurrences stems from the permanent alignment of the molecules [see the first term in the right-hand side of Eq. (15)]. It increases, as well as the amplitude of the revivals, when high values of J are populated. A significant value of the permanent alignment is reached when $\bar{J}\gg|M|$, where $\bar{J}$ is an average value of the field-populated J-states and M is the magnetic quantum number [21].

The observed signal is compared with the numerical simulation of the Schrödinger equation performed at 296 K.

Section II describes in detail how the polarization signal is related to the molecular and field parameters. The calculated signal intensity, according to Eq. (1) with $C=0$, is depicted in Fig. 2. The ordinate scale is adjusted so that the calculated amplitude is comparable with the observed signal. The calculation uses an effective pump-peak intensity of 40 TW/cm^2, for which the structural shape of the transients reproduces the observation. This intensity is consistent with the measured value, considering that volume effects are not included in the theoretical model. In fact, an averaging of Eq. (1) over the spatial profile of the laser would result in using larger intensity in the simulation, closer to the measured intensity. We remark that damping of the molecular response due to collisional mechanisms is insignificant in the experimental conditions explored in Fig. 2. The upper graph of Fig. 2 displays the corresponding value of $\langle\cos^2\theta\rangle$. Its horizontal scaled axis is shifted by the vertical offset 1/3 corresponding to the isotropic value of $\langle\cos^2\theta\rangle$. The figure shows that each recurrence results from alignment ($\langle\cos^2\theta\rangle > 1/3$) and planar delocalization ($\langle\cos^2\theta\rangle < 1/3$) of the molecular axis. In the first case, the angular distribution is squeezed along the electric field direction, whereas it is flattened around the plane perpendicular to the field axis, in the second case. The highest value of $\langle\cos^2\theta\rangle$ is observed for the third transient ($3T_r/4$) at $\tau \approx 32.1$ ps. It is consistent with the polarization signal being maximal for the third recurrence (see the lower graph of Fig. 2). Maximum alignment, observed around $\tau = 3T_r/4$, and planar delocalization, observed around $\tau = T_r/4$, comes from efficient temporal rephasing of the wave packet, as shown in the model developed in Sec. II. For the other transients ($T_r/2$ and T_r) the partial rephasing results in less confinement of the angular distribution. Between recurrences, the rotational phase distribution changes such that the rotational wave functions nearly average out, giving rise to a permanent alignment.

The relevant quantity that characterizes the alignment of an ensemble of molecules is, according to Eq. (5), the thermal average of $\langle\cos^2\theta\rangle$. For a given temperature, the average is calculated over the rotational states initially populated before the laser interaction. Because the initial states are not coherently related through the thermal excitation, the averaging mechanism tends to smooth out the angular distribution of the single molecule. Therefore, reducing the temperature of the molecular sample makes larger alignment possible [14]. This is confirmed by a study performed at low temperature ($\approx$60 K) in a molecular jet of CO_2. The detection is heterodyned for the reason explained in Sec. III. The polarization signal is shown in Fig. 3 together with the results of the theoretical model according to Eq. (1) with the constant C adjusted to the background signal. We note that the signal noise is larger in the jet experiment than in the static cell, due to the low number density of the gas expansion and the shorter interaction length in the jet. Since heterodyne detection provides the phase of the signal-field, the transient shapes tell about whether the molecule is aligned or planarly delocalized. In the case of Fig. 3, the measurement performed close to zero delay indicates that the constant C is negative. Therefore, the peak and the valley of each transient are identified as planar delocalization and alignment of the

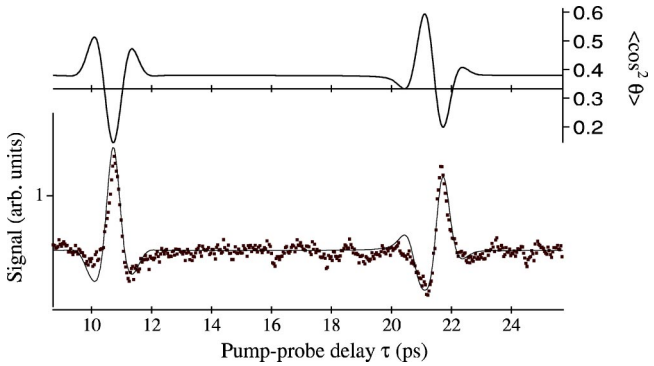

FIG. 3. Lower graph: heterodyne signal (doted curve) versus pump-probe delay τ recorded in a supersonic jet of CO_2. Numerical simulation of Eq. (1) (full curve) performed at 60 K for a peak intensity of 30 TW/cm^2. Upper graph: corresponding values of $\langle\cos^2\theta\rangle$.

molecules, respectively. A net improvement of the alignment ($\langle\cos^2\theta\rangle \approx 0.59$, $\tau \approx 21.11$ ps) and planar delocalization ($\langle\cos^2\theta\rangle \approx 0.14$, $\tau \approx 10.7$ ps) is observed at low temperature. These numbers should be compared with the $\langle\cos^2\theta\rangle$ values calculated in Fig. 2 for a larger intensity. By increasing the cooling, a much higher degree of alignment can be in principle achieved, although it was not possible with the present polarization technique to detect its effect due to the resulting low gas number density. This is illustrated in Fig. 4, where a simulation at 2 K shows a peak value of $\langle\cos^2\theta\rangle \approx 0.86$.

B. Relative calibration

In the preceding section, the molecular alignment was quantified by fitting the numerical simulation to the temporal shape of the observed transients (see Figs. 2 and 3). In this procedure, the signal amplitude was parameterized with an adjusted scale factor from which no information was extracted. In the present section, we describe a method that allows recovering the degree of alignment from the measured signal amplitude. The polarization signal is calibrated with reference to measurements performed in Argon.

The relative calibration is performed along the following protocol. The polarization signal is produced in a static cell

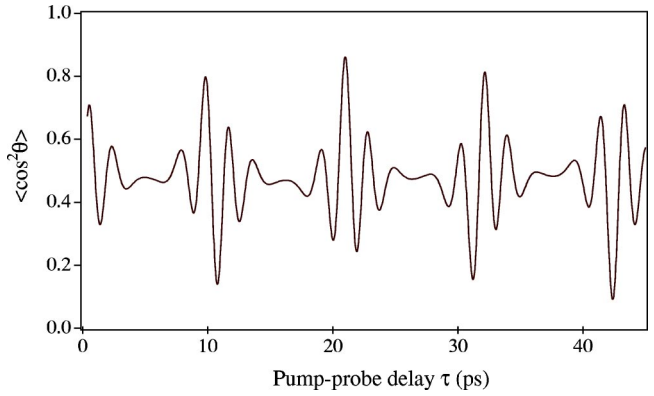

FIG. 4. Numerical simulation of $\langle\cos^2\theta\rangle$ as a function of the time delay for $T=2$ K and $I=30$ TW/cm^2.

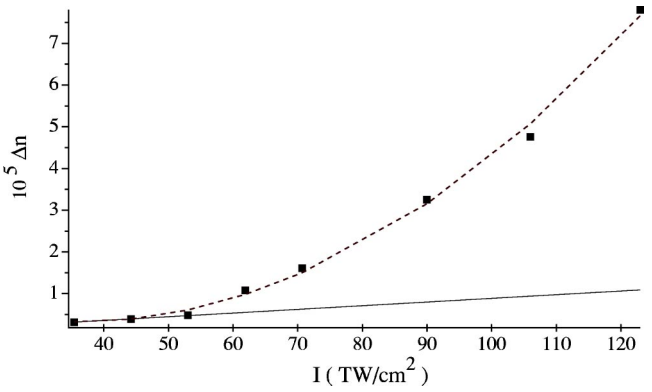

FIG. 5. Variation of the refractive index of Argon measured at different laser intensities I (squares). Numerical fit with a second-order polynomial function in the intensity (dashed curve). Quadratic field dependence $\Delta n = \overline{n_2} I$ (full curve).

filled with Argon and recorded at different pump-laser intensities. For atoms, the induced birefringence is solely due to the electronic nonlinear response, which is much faster than the pulse duration of the laser used in the experiment. The pump-probe signal is thus the third-order autocorrelation of the laser, whose magnitude depends on the laser intensities (pump and probe) and the electronic response. The electronic deformation results in a birefringence signal-field proportional to the refractive index difference Δn [see Sec. II, Eqs. (1) and (2)]. For low field intensities I, the nonlinear dependence of the refractive-index is quadratic with the field amplitude and $\Delta n = \overline{n_2} I$, where $\overline{n_2}$ is the lowest nonlinear order. Considering the value of $\overline{n_2}$ for Argon [29], we therefore calibrate the signal intensity in terms of $(\Delta n)^2$ by performing experiments in the low field regime. The graph of Fig. 5 shows the value of Δn (squares) measured for different laser intensities. The expected value of Δn assuming a quadratic field dependence (with $\overline{n_2}$ taken from Ref. [29]) is also indicated (full curve). The calibration has been performed for $I < 50$ TW/cm^2, where Δn is proportional to the square of the field, i.e., to the intensity I. This enables one to determine the calibrated constant κ introduced in Eq. (1). For $I > 50$ TW/cm^2, higher nonlinear orders of the refractive index must be considered. It is shown in Fig. 5 that Δn can be fitted with a second-order polynomial function in I (dashed curve) up to $I = 120$ TW/cm^2.

Using the same probe pulse as the one used for the calibration in Argon, i.e., the same intensity and spatial profile, the experiment is performed with CO_2. The pump-probe signal is converted into the variation of the refractive index $(\Delta n)^2$ through the calibration factor κ determined before. After the pump-pulse extinction, the change of the refractive index stems exclusively from the molecular orientation induced by the optical field. In this case, Δn is related to $\langle \cos^2 \theta \rangle - \frac{1}{3}$ through Eq. (4) of Sec. II.

The validity of the relative calibration method is demonstrated in Fig. 6. The plots are displayed in a temporal window centered on the first (a, d, g), the second (b, e, h), and the third transient (c, f, i). The transients are recorded for three different pump intensities. The experimental data (full curve) are displayed with the vertical axis scaled in units of $|\langle \cos^2 \theta \rangle - \frac{1}{3}|$. They are compared with the simulation of the Schrödinger equation (dotted curve). As mentioned in Sec. IV A, the calculation of Eq. (1) is performed with an effective intensity that is lower than the measured pump-laser intensity by 30%. As shown, the agreement between the calibrated data and the result of the simulation is remarkable.

The intensity dependence of the polarization signal is dominated by the structural change of the recurrence when the field strength is increased. This is interpreted as follows. First, the width of the distribution of the wave packet in the J-space increases with the laser intensity. The revivals become thus more localized in time producing narrow transients. Second, in case of homodyne detection (Figs. 2 and 6), the detected field is proportional to the difference between $\langle \cos^2 \theta \rangle$ and its isotropic value $\frac{1}{3}$. Therefore the shape of the transients becomes more asymmetric as the permanent alignment increases (see Fig. 6). The situation is different for heterodyne detection (Fig. 3), where the field amplitude is proportional to $\langle \cos^2 \theta \rangle - \frac{1}{3} + C'$, with $C' = 4n\epsilon_0 C / 3N\Delta\alpha$. For $|C'| \gg \frac{1}{3}$ the transient shape is insensitive to the permanent alignment and the asymmetry remains unchanged with the laser intensity [21]. The progressive effect of permanent alignment with the field strength is observed by comparing the background signals of Figs. 6 recorded at different intensities.

The concomitant ionization process that depletes the population of the neutral molecules, limits the maximum alignment achievable at a given temperature. As the laser intensity approaches the ionization saturation intensity, the observed transients exhibit structural shapes that become relatively insensitive to the field strength. The onset of saturation first affects the molecules in the middle of the laser focus; the ionized molecules cannot contribute anymore to the polarization signal and hence to the modification of the shape of the transients. Although saturation is reached at the center of the beam, the surrounding molecules, that experience lower intensities, still contribute to the signal up to the limit where they are ionized as well. This "volume effect" keeps on until the pump laser intensity saturates the whole volume seen by the probe-beam. Beyond this point, no molecules survive to the laser intensity and only the remaining ions can in principle be aligned and detected. The saturation effect is illustrated in Fig. 7, where the intensity adjusted in the simulation of the third transient is plotted versus the measured laser intensity. The simulation, based on Eq. (1), does not include the ionization mechanism. Inspection of the data clearly indicates the onset of saturation around a laser intensity of about 100 TW/cm^2, where the transient shape starts saturating. Above this intensity, the adjusted intensity must be taken smaller in order for the simulation to reproduce the observed transient shape. The measured intensity corresponds to the energy averaged over the focus size, and therefore underestimates the peak intensity (at the beam center) by about a factor 2. As a result, the mentioned value (100 TW/cm^2) translates to a peak intensity of about 2.0×10^{14} W/cm^2, which is consistent with the ionization saturation intensity of CO_2 at 800 nm (2.4×10^{14} W/cm^2 [30]). Between 200 and 250 TW/cm^2, the transient shape remains unchanged with the intensity. No signal amplitude saturation,

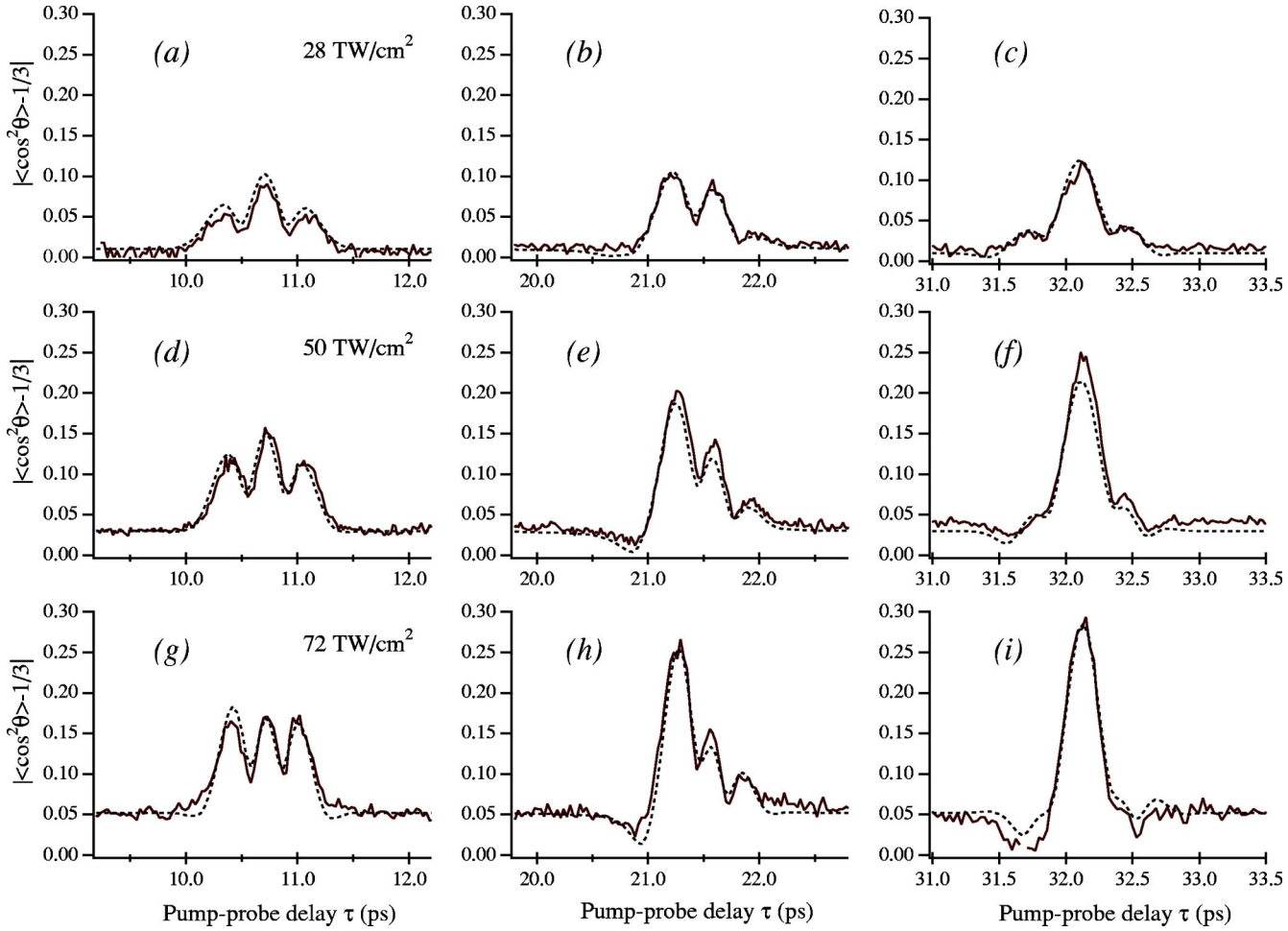

FIG. 6. Calibrated homodyne signals (full curves) recorded in a static cell of CO_2 for different temporal windows and laser intensities. The ordinate axes indicate the value of $|\langle\cos^2\theta\rangle-\frac{1}{3}|$ supplied by the calibration achieved in Ar (see text). The numerical simulations (dotted curves) is performed at different effective intensities: $I=28$ TW/cm^2 (a, b, and c), 50 TW/cm^2 (d, e, and f), 72 TW/cm^2 (g, h, and i).

nor *a fortiori* depletion of the transient signal, is observed at the highest intensities used in the present work. This indicates that the saturation of the probed volume cannot be achieved under the investigated intensity regime. This argument is supported by the fact that no signature from ionic molecules is observed.

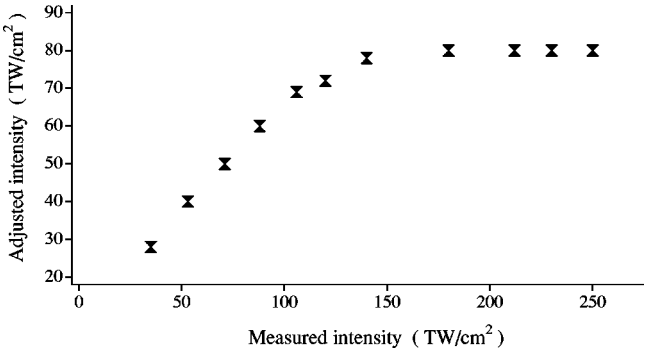

FIG. 7. Adjusted intensity on the shape of the third alignment transient as a function of the measured laser intensity. The large discrepancy between theoretical and experimental values at high intensities stems from saturation of the alignment due to ionization.

V. CONCLUSION

Impulsive alignment of the CO_2 molecule has been monitored using a nonintrusive weak-field polarization spectroscopy technique. The experiments have been conducted at room temperature (in a static cell) and at low temperature (in the free expansion of a molecular jet) with homodyne and heterodyne detection, respectively. The results have been analyzed with two complementary methods, *shape based analysis* and *relative calibration*. The first one consists in comparing the raw data to the predictions of the theoretical model, based on the resolution of the Schrödinger equation, which allows to extract the expected $\langle\cos^2\theta\rangle$ value. The simulation requires a slight adjustment of the strong-field intensity around the measured value in order to fit the observations. With this procedure, only the structural shape of transients provides information about the alignment, since the amplitude is adjusted by a free parameter in the model. The quality of the experimental data allows an accurate characterization of the alignment at low and high temperatures. The analysis is confirmed and completed by the use of the second method which provides a straightforward evaluation of $|\langle\cos^2\theta\rangle-\frac{1}{3}|$, based on the calibration of the detection sys-

tem with reference to measurements made in an atomic gas. The analysis of the calibrated measurements is checked by considering the results predicted by the numerical simulation of the Schrödinger equation. The recurrent alignment is investigated for different intensities, up to a limit where saturation of the ionization sets-on. At high laser intensities, the limitation in the alignment is shown to be correlated to the ionization depletion of neutral molecules in the probed volume.

ACKNOWLEDGMENTS

The authors wish to acknowledge the financial support by the Conseil Régional de Bourgogne, by the CNRS, and by the ACI *photonique* from the French Ministry of Research.

APPENDIX: THE BEAT PHASES IN A SOLVABLE MODEL

In this Appendix, we show that the phases $\Delta\theta_J^{J_0,M_0}$ of Eq. (16) are approximately $\pm\pi/2$. This can be understood from the approximate model developed in Ref. [14] for $J_0=0$, which we extend for a thermal ensemble. It is formulated in the impulsive regime [31] where the propagator in the normalized time unit $s=Bt/\hbar$ reads

$$U(s,s_i) = e^{i\gamma_\perp \mathcal{A}(s-s_i)} e^{-iJ^2 s} e^{i2\zeta\cos^2\theta} e^{iJ^2 s_i} \tag{A1}$$

with $s_i=Bt_i/\hbar$, $s \geqslant s_f=Bt_f/\hbar$, $\zeta=\mathcal{A}\Delta\gamma/2=\mathcal{E}_0^2\Delta\alpha\int_{t_i}^{t_f}dt\ \Lambda_p(t)/(8\hbar)$, and $\mathcal{A}=\frac{B}{\hbar}\int_{t_i}^{t_f}dt\ \Lambda_p(t)$ the normalized area of the pump intensity envelope. The term $e^{i\gamma_\perp\mathcal{A}(s-s_i)}$ giving an additional phase independent of J will not affect the quantity $\langle\cos^2\theta\rangle_{J_0,M_0}(t)$. The approximate model is additionally constructed by substituting $\cos^2\theta$ by an operator $\mathcal{C}$ with matrix elements $\langle J,M_0|\mathcal{C}|J,M_0\rangle=1/2$, $\langle J+2,M_0|\mathcal{C}|J,M_0\rangle=1/4$, and $\langle J',M_0|\mathcal{C}|J,M_0\rangle=0$ for $J'>J+2$, for all J,M_0. This leads to

$$e^{i2\zeta\mathcal{C}} = e^{i2\zeta} \sum_{J,J'\text{even}} u_J^{J'}(\zeta)|J\rangle\langle J'| \tag{A2}$$

with, for $\zeta>0$ and defining $a_n=J/2-J'/2+1+2n$,

$$u_J^{J'}(\zeta) = e^{i\pi/4(J-J')}\frac{2}{\zeta}\sum_{n=0}^{J'/2}(-1)^n a_n \mathcal{J}_{a_n}(\zeta). \tag{A3}$$

This amounts to substituting

$$\alpha_{J,M_0}=1/2,\ \beta_{J,M_0}=1/4 \tag{A4}$$

in Eq. (15). We obtain in this approximation

$$\langle\cos^2\theta\rangle_{0,0}(t) = \frac{1}{2}+\frac{2}{\zeta^2}\sum_{J\text{even}}(J/2+1)\mathcal{J}_{J/2+1}(\zeta)\times(J/2+2)\mathcal{J}_{J/2+2}(\zeta)\sin(\omega_J t), \tag{A5}$$

where $\mathcal{J}_\alpha(\zeta)$ is the Bessel function of order α and of argument ζ. We thus obtain for this model the following phases for Eq. (15):

$$\Delta\theta_J^{0,0} = \frac{\pi}{2}(\text{sgn}[\mathcal{J}_{J/2+1}(\zeta)]-\text{sgn}[\mathcal{J}_{J/2+2}(\zeta)]-1) = \pm\pi/2 \tag{A6}$$

with the sign function $\text{sgn}(x)=+1$ if $x\geqslant 0$ and -1 otherwise. Detailed analysis of this expression shows that since the Bessel functions $\mathcal{J}_{J/2+1}(\zeta)$ have the same sign for all even J for $\zeta\lesssim 3.83$, we have only in this case $\Delta\theta_J^{0,0}=-\pi/2$ for all even J. In this case, the components of the sines have all the same sign (positive) and will thus accumulate for all J only around $t=t_p\equiv pT_r/4=p\pi/4B$, with p an integer: One obtains for $\langle\cos^2\theta\rangle_{0,0}$ a value of 0.5 at $t=t_0=0$ and at $t=t_2=T_r/2$, the main maximum at $t=t_3=3T_r/4$ $[\sin(\omega_J t)=1]$, and the main minimum at $t=t_1=T_r/4$ $[\sin(\omega_J t)=-1]$. Around $t=T_r/2$, one obtains a local maximum (for $t\lesssim T_r/2$) and a local minimum (for $t\gtrsim T_r/2$) that can be evaluated by expanding $\sin(\omega_J t)$. For $\zeta>3.83$, the main contributions of $\langle\cos^2\theta\rangle_{0,0}(t)$ occur with the phase $-\pi/2$, which explains the remarkable efficiency of the alignment for strong field. This expression (A5) can be extended for a thermal ensemble and leads to a similar result that the phases $\Delta\theta_J^{J_0,M_0}$ are approximately $\pm\pi/2$ with a dominant contribution occurring for $-\pi/2$. Indeed we find in the limit of strong field (large ζ) at time t_3 (where even J_0 has been considered)

$$\langle\cos^2\theta\rangle_{J_0,M_0}(t_3) \rightsquigarrow \frac{1}{2}+\sum_{n=0}^{J_0/2}(-1)^n S_n \tag{A7}$$

(where the wiggly arrow indicates that the left part of the equation asymptotically tends to the right part), with

$$S_n = \frac{2}{\zeta^2}\sum_{k=1}^{\infty}[k\mathcal{J}_k(\zeta)][(k+2n+1)\mathcal{J}_{k+2n+1}(\zeta)]. \tag{A8}$$

We obtain the approximate asymptotic values $S_0\to 0.42$, $S_1\to 0.086$, $S_2\to -0.013$, $S_3\to 0.006,\ldots,\lim_{n\to\infty}S_n=0$, which shows that the main contributions are associated to the phase $\Delta\theta_J^{J_0,M_0}=-\pi/2$.

[1] R. A. Bartels, N. L. Wagner, M. D. Baertschy, J. Wyss, M. M. Murnane, and H. C. Kapteyn, Opt. Lett. **28**, 346 (2003).
[2] N. Hay, R. Velotta, M. Lein, R. de Nalda, E. Heesel, M. Castillejo, and J. P. Marangos, Phys. Rev. A **65**, 053805 (2002).
[3] Z. X. Zhao, X. M. Tong, and C. D. Lin, Phys. Rev. A **67**, 043404 (2003).
[4] I. V. Litvinyuk, K. F. Lee, P. W. Dooley, D. M. Rayner, D. M. Villeneuve, and P. B. Corkum, Phys. Rev. Lett. **90**, 233003 (2003).
[5] T. Seideman, J. Chem. Phys. **111**, 4397 (1999).
[6] B. Friedrich and D. Herschbach, Phys. Rev. Lett. **74**, 4623 (1995).
[7] H. Stapelfeldt and T. Seideman, Rev. Mod. Phys. **75**, 543

(2003).
[8] J. J. Larsen, K. Hald, N. Bjerre, H. Stapelfeldt, and T. Seideman, Phys. Rev. Lett. **85**, 2470 (2000).
[9] H. Stapelfeldt, H. Sakai, E. Constant, and P. B. Corkum, Phys. Rev. Lett. **79**, 2787 (1997).
[10] J. J. Larsen, H. Sakai, C. P. Safvan, I. Wendt-Larsen, and H. Stapelfeldt, J. Chem. Phys. **111**, 7774 (1999).
[11] D. Normand, L. A. Lompre, and C. Cornaggia, J. Phys. B **25**, L497 (1992).
[12] J. Ortigoso, M. Rodriguez, M. Gupta, and B. Friedrich, J. Chem. Phys. **110**, 3870 (1999).
[13] K. Hoshina, K. Yamanouchi, T. Ohshima, Y. Ose, and H. Todokoro, J. Chem. Phys. **118**, 6211 (2003).
[14] T. Seideman, J. Chem. Phys. **115**, 5965 (2001).
[15] F. Rosca-Pruna and M. J. J. Vrakking, Phys. Rev. Lett. **87**, 153902 (2001).
[16] F. Rosca-Pruna and M. J. J. Vrakking, J. Chem. Phys. **116**, 6567 (2002).
[17] F. Rosca-Pruna and M. J. J. Vrakking, J. Chem. Phys. **116**, 6579 (2002).
[18] P. W. Dooley, I. V. Litvinyuk, K. F. Lee, D. M. Rayner, M. Spanner, D. M. Villeneuve, and P. B. Corkum, Phys. Rev. A **68**, 023406 (2003).
[19] E. Péronne, M. D. Poulsen, C. Z. Bisgaard, H. Stapelfeldt, and T. Seideman, Phys. Rev. Lett. **91**, 043003 (2003).
[20] J. G. Underwood, M. Spanner, M. Y. Ivanov, J. Mottershead, B. J. Sussman, and A. Stolow, Phys. Rev. Lett. **90**, 223001 (2003).
[21] V. Renard, M. Renard, S. Guerin, Y. T. Pashayan, B. Lavorel, O. Faucher, and H. R. Jauslin, Phys. Rev. Lett. **90**, 153601 (2003).
[22] M. Morgen, W. Price, L. Hunziker, P. Ludowise, M. Blackwell, and Y. Chen, Chem. Phys. Lett. **209**, 1 (1993).
[23] J. R. Lalanne, A. Ducasse, and S. Kielich, *Laser-Molecule Interaction: Laser Physics and Molecular Nonlinear Optics* (Wiley, New York, 1996).
[24] C. M. Dion, A. Keller, O. Atabek, and A. D. Bandrauk, Phys. Rev. A **59**, 1382 (1999).
[25] A. Keller, C. M. Dion, and O. Atabek, Phys. Rev. A **61**, 023409 (2000).
[26] T. Seideman, Phys. Rev. Lett. **83**, 4971 (1999).
[27] H. Ashkenas and F. Sherman, in *Rarefied Gaz Dynamics*, edited by J. de Leeuw (Academic Press, New York, 1966), Vol. II, pp. 84–105.
[28] Minhaeng-Cho, Mei-Du, N. F. Scherer, G. R. Fleming, and S. Mukamel, J. Chem. Phys. **99**, 2410 (1993).
[29] E. T. J. Nibbering, G. Grillon, M. A. Franco, B. S. Prade, and A. Mysyrowicz, J. Opt. Soc. Am. B **14**, 650 (1997), and references therein.
[30] C. Cornaggia and P. Hering, Phys. Rev. A **62**, 023403 (2000).
[31] N. E. Henriksen, Chem. Phys. Lett. **312**, 196 (1999).